Krauskopf, B., Erzgraber, H., & Lenstra, D. (2006). Dynamics of semiconductor lasers with filtered optical feedback.

Early version, also known as pre-print

Dynamics of semiconductor lasers with filtered optical feedback

B. Krauskopf[a,b], H. Erzgräber[b], and D. Lenstra[b,c]

[a]Department of Engineering Mathematics, University of Bristol, UK
[b]Natuurkunde en Sterrenkunde, Vrije Universiteit Amsterdam, The Netherlands
[c]COBRA Research Institute, Technische Universiteit Eindhoven, The Netherlands

ABSTRACT

In the filtered optical feedback (FOF) scheme a part of the emission of the laser is spectrally filtered, for example by a Fabry-Pérot filter, and than fed back into the laser. If a semiconductor laser is subject to such delayed FOF qualitative different types of oscillations are possible: the well known relaxation oscillations and, more remarkably, frequency oscillations. We explain how the continuous wave operation of the FOF laser — the external filtered modes — lose their stability and the different types of oscillations arise due to the presence of the filter. This study is restricted to the case of a narrow filter. This means that there are only a few external filtered modes within the width of the filter, so that the influence of the feedback phase can be studied explicitly.

Keywords: filtered optical feedback, delay, external filtered modes, bifurcation analysis, numerical continuation

1. INTRODUCTION

Semiconductor lasers (SLs) are very sensitive to external perturbations. This is mainly because of their high intrinsic gain, which means that even small perturbations are amplified strongly. Different types of external influences on the dynamics of SLs have been considered in the past, including injection, coherent and incoherent optical feedback, optoelectronic feedback, and mutual coupling. As entry points into nonlinear dynamics of semiconductor lasers with optical injection or feedback see, for example, Refs. [1–4].

Filtered optical feedback (FOF) is a type of coherent feedback in which the light is spectrally filtered before it re-enters the laser[5–9]; see Fig. 1 . Specifically, a part of the emission of the laser is directed through a feedback loop where it is spectrally filtered, for example by a Fabry-Pérot filter, and then fed back into the laser. Due to the finite propagation time of the light, the feedback field accumulates a non-negligible time delay. This external feedback system has several parameters that influence the overall dynamics. First, there are the delay time and the feedback rate, which are control parameters in any type of delayed feedback. Specific for coherent delayed feedback there is also the feedback phase. Particular to FOF as studied here, there are additional control parameters, namely the detuning between the filter center frequency and the solitary laser frequency, and the linewidth of the filter.

The study presented here is restricted to the case of a narrow filter, which means that only a few external filtered modes (EFMs), the system's CW-states, are within the width of the filter. In this situation the feedback phase plays a key role in organizing the structure of the EFMs. We describe the FOF system by a set of rate

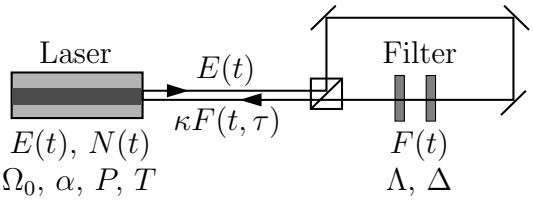

Figure 1. Sketch of the system with the semiconductor laser and a Fabry-Pérot filter made of two semi-transparent mirrors in the feedback loop.

equations with delay and use advanced bifurcation techniques to find and follow EFMs and different types of bifurcating oscillations. Depending on the parameters, these oscillations may either be the well-known relaxation oscillations or pure frequency oscillations. Apart from their different typical time scale in the order of the delay time, frequency oscillations are also quite different from relaxation oscillations in another respect: the laser frequency oscillates while the intensity of the laser is almost constant.[8,10] An analytical study of these different oscillations is presented in Ref. [11], where a reduced model for weak feedback is analyzed and compared with the full rate equation model.

2. RATE EQUATION MODEL

We describe the FOF laser system by a set of rate equations for the slowly varying complex envelope $E(t)$ of the laser field and for the inversion $N(t)$ of the laser (with respect to its inversion at threshold). Furthermore, we model the slowly varying complex envelope $F(t)$ of the filtered feedback field, where the line shape of the filter is approximated by a single Lorentzian. Details about the model and its validity can be found in, *e.g.*, Refs. [5, 6]. If time t is measured in units of the photon life time (typically in the order of 10 ps for semiconductor lasers) the rate equations can be written in dimensionless form as

$$\frac{dE}{dt} = (1+i\alpha)N(t)E(t) + \kappa F(t,\tau) \tag{1}$$

$$T\frac{dN}{dt} = P - N(t) - (1+2N(t))|E(t)|^2 \tag{2}$$

$$\frac{dF}{dt} = \Lambda E(t-\tau)e^{-iC_p} + (i\Delta - \Lambda)F(t)\,. \tag{3}$$

Here τ is the delay time that arises from the finite propagation time of the light in the feedback loop, and κ is the feedback rate. The feedback phase C_p measures the detuning between the filter and the external mode structure induced by the feedback loop, whereas Δ is the detuning between the filter center frequency Ω_F and the solitary frequency Ω_0 laser, that is, $C_p = \Omega_0\tau$ and $\Delta = \Omega_F - \Omega_0$. The parameter Λ is the filter width (half width at half maximum). The material properties of the laser are given by the linewidth enhancement factor α and the electron life time T, and P is the pump current. Throughout, we choose the values of the parameters as given in Table 1.

3. EFMS AND THE INFLUENCE OF THE FEEDBACK PHASE

The external filtered modes are solutions of Eq. (1)–(3) of the form

$$(E(t)\,, N(t)\,, F(t)) = (R_s e^{i\omega_s t}\,, N_s\,, F_s e^{i\omega_s t + i\phi}) \tag{4}$$

Table 1. Meaning of the parameter and their values.

symbol	laser parameter	value
α	linewidth enhancement factor	5
T	electron life time	100
P	pump parameter	3.5
τ	external round-trip time	500
κ	feedback rate	$[0, 0.035]$
C_p	feedback phase	$\{0; 2/6\pi; 4/6\pi; 6/6\pi; 8/6\pi; 10/6\pi\}$
Λ	filter width (HWHM)	0.007
Δ	filter detuning	selected values in $[-0.0595, 0.0595]$

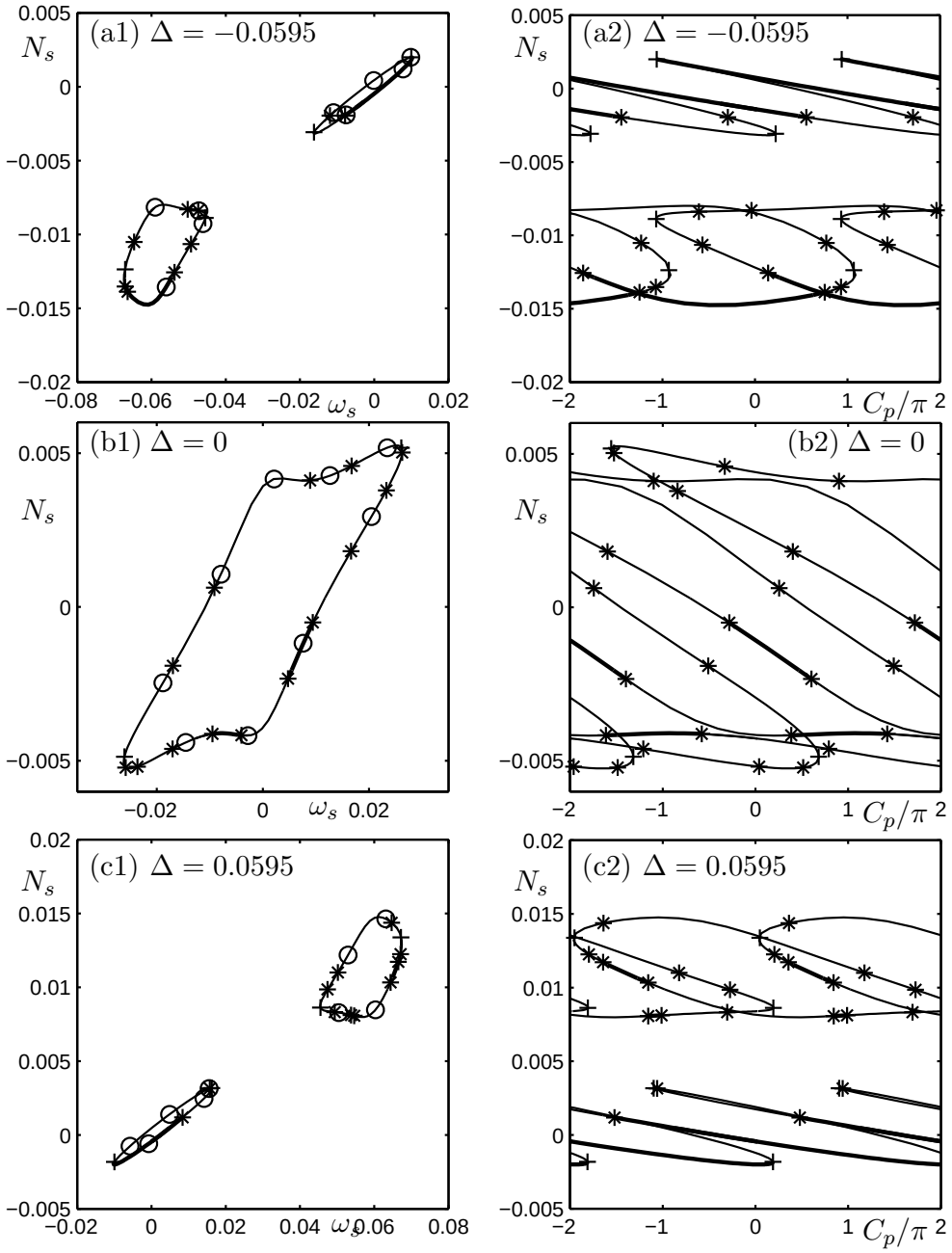

Figure 2. The EFMs in the (ω_s, N_s)-projection (left column) and in the (C_p, N_s)-projection (right column) for different values of the detuning Δ as indicated in the panels. For fixed C_p a finite number of EFMs exists (indicated by circles ($\circ$) in the (ω_s, N_s)-projection); as C_p is changed they trace out the underlying curve. Stable parts of the branches are plotted thick, saddle-node bifurcations are indicated as plusses ($+$) and Hopf bifurcations by stars ($*$).

for fixed real numbers R_s, N_s, F_s, ω_s and ϕ. A detailed analytical treatment of the EFMs can be found in Refs. [12, 13].

In this paper we discuss how the EFMs depend on the feedback rate κ and the feedback phase C_p. Furthermore, we consider their stability regions in the (κ, C_p)-plane. To this end we use the numerical continuation software DDE-BIFTOOL.[14]

Figure 2 shows the EFMs in the (ω_s, N_s)-projection and in the (C_p, N_s)-projection for three different values of detuning Δ. In panel (a1), for $\Delta = -0.0595$, two separated EFM components can be found — one around the solitary laser frequency for which $\omega_s \approx 0$, and a second one around the center frequency of the filter, for which $\omega_s \approx -0.0595$. Note that both EFM components feature stable EFMs. The EFMs for $C_p = 0$ are indicated as circles ($\circ$) in Fig. 2(a1). A one-parameter bifurcation diagram of the EFMs in the (C_p, N_s)-projection is shown in Fig. 2(a2). Stable regions on the curves are plotted thick, saddle-node bifurcations are indicated by plusses ($+$) and Hopf bifurcations by stars ($*$). As C_p is decreased in the (ω_s, N_s)-projection, EFMs are born in pairs in saddle-node bifurcations in the low-inversion region of the respective curve. They trace out the respective EFM component, one on the lower part and one on the upper branch. Eventually, they disappear in pairs in saddle-node bifurcations in the high-inversion region. EFMs can be stable in certain C_p intervals, which are plotted thick; already unstable EFMs may encounter further Hopf bifurcations, as is indicated by stars ($*$).

As the detuning is increased to zero the two separate EFM components in the (ω_s, N_s)-projection merge into a single EFM component, such as the one in Fig. 2(b1) for $\Delta = 0$. This happens when a saddle singularity is passed; see Refs. [12, 13]. Also in the (C_p, N_s)-projection of Fig. 2(b2) there is now only one single, infinitely long curve of EFMs.

For even larger detuning there are again two EFMs components, but now the EFMs around the filter frequency are on the negative side with respect to the solitary laser frequency. In the (ω_s, N_s)-projection of Fig. 2(c1) one EFM component is around $\omega_s \approx 0$ (the solitary laser frequency) and the second around $\omega_s \approx 0.0595$ (the center frequency of the filter). Again both EFM components feature stable EFMs. Note that the images for positive and negative Δ, Figs. 2(a) and (c), are not each others symmetric counterparts due to the influence of the line-width enhancement factor α.

4. INFLUENCE OF THE DETUNING

Figure 3 shows one-parameter bifurcation diagrams of the EFMs in the (κ, N_s)-projection for increasing values of the detuning from $\Delta = 0$ to $\Delta = 0.0595$. In black are the branches of EFMs, thick parts are stable and thin parts are unstable. At zero feedback ($\kappa = 0$) there exists only the solitary laser modes, which gives rise to a distinct branch of EFMs. This branch is initially stable. Under the influence of increasing feedback the inversion N_s changes and, eventually, the EFM destabilizes in a Hopf bifurcation. Additional EFMs are created in pairs in saddle-node bifurcations. One of the bifurcating EFMs may initially be stable but, when κ is increased, then destabilizes in a Hopf bifurcation.

Figure 3 shows the branches for the fixed feedback phase of $C_p = 0$. When the feedback phase C_p is changed the branches move, giving the same picture after C_p has been changed over 2π. In this process the saddle-node bifurcations trace out the gray curve in (κ, N_s)-projection. In other words, the gray curve in each panel of Fig. 3 is the branch of saddle-node bifurcations in the (κ, N_s)-projection as parameterized by the feedback phase C_p.

For $\Delta = 0$, when the filter frequency coincides with the laser frequency, the gray saddle-node branch reaches almost to zero feedback, $(\kappa, N_s) = (0, 0)$, where it has a turning point (a minumim with respect to κ); see Fig. 3(a). As the detuning is increased, this minimum stays approximately at the same inversion (around $N_s = 0$) but moves towards higher feedback rates. This means that more feedback is needed to create an additional EFM pair. Furthermore, the saddle-node branch develops two more turning points — a local maximum and another (local) minimum with respect to κ; see Fig. 3(c). The EFMs in the low-inversion part are around the solitary laser frequency. The EFMs in the high-inversion part are around the center frequency of the filter. Note that positive Δ means that the solitary laser frequency is smaller than the filter frequency. Because of the α-parameter this blue shift is associated with an increase of the inversion and with a decrease of the intensity, respectively. The resulting two EFM components (one around the solitary laser frequency and one around the filter frequency) separate further when the detuning is increased. This is expressed in Fig. 3 by the fact that the local maximum moves to larger feedback rates. As a result, in Fig. 3(d)–(f) there is only one EFM component around the solitary laser for κ below the local minumum of the saddle-node curve. As κ is increased beyond this value, the second EFM component appears around the filter frequency. Eventually, when κ moves past the local maximum of the saddle-node curve then the two EFM components merge into a single EFM component. For an analytical treatment of EFM components see Refs. [12, 13].

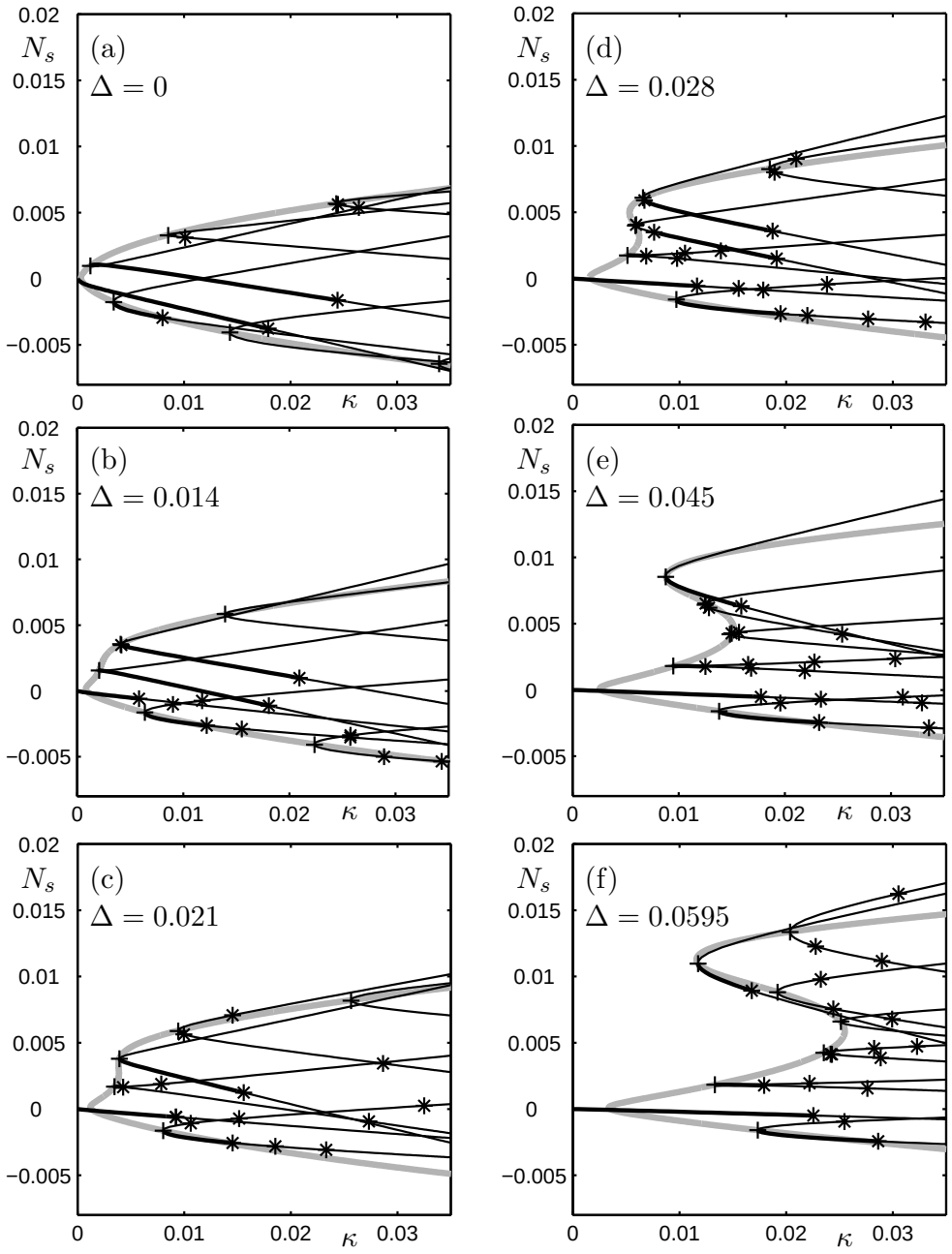

Figure 3. The EFMs in the (κ, N_s)-projection for different detunings Δ as indicated in the panels. Stable parts of the branches are plotted thick, saddle-node bifurcations are indicated as plusses (+) and Hopf bifurcations by stars (∗); the gray curve is traced out by the saddle-node bifurcations as C_p is changed.

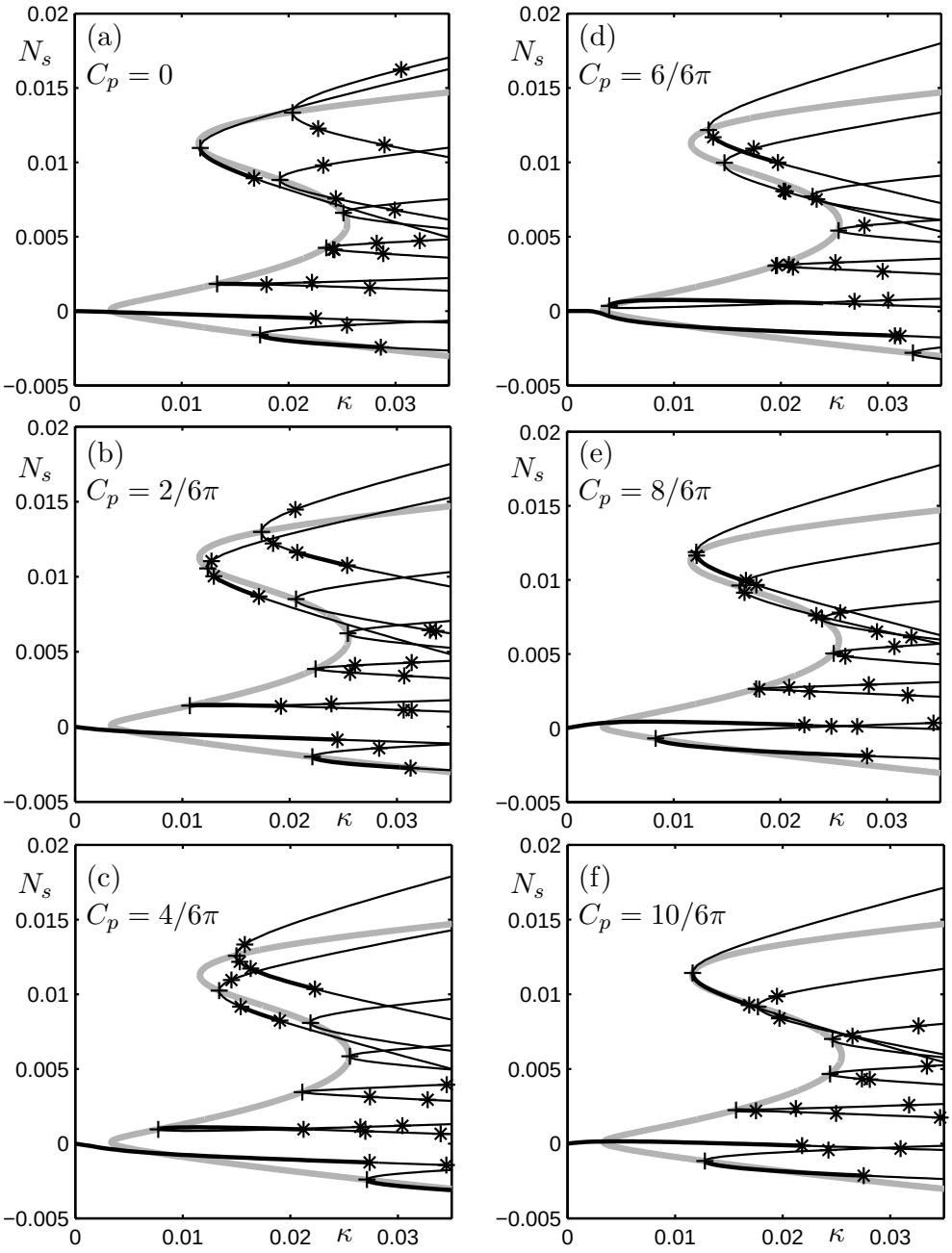

Figure 4. The EFMs for positive detuning $\Delta = 0.0595$ in the (κ, N_s)-projection for different values of the feedback phase C_p as indicated in the panels. Stable parts of the branches are plotted thick, saddle-node bifurcations are indicated as plusses (+) and Hopf bifurcations by stars (∗); the gray curve is traced out by the saddle-node bifurcations as C_p is changed.

Figure 4 shows one-parameter bifurcation diagrams of the EFMs in the (κ, N_s)-projection for positive detuning of $\Delta = 0.0595$ and for different values of the feedback phase $C_p = 0$. Again in black are the branches of EFMs, where thick parts are stable and thin parts are unstable. The gray curve is the branch of saddle-node bifurcations, which is parametrized by C_p. Note that Fig. 4(a) is identical to Fig. 3(f). When C_p is changed over 2π then every EFM branch has moved exactly to the position of its next neighbor. The saddle-node bifurcations where the branches start trace out the grey saddle-node curve in the process. To trace out the

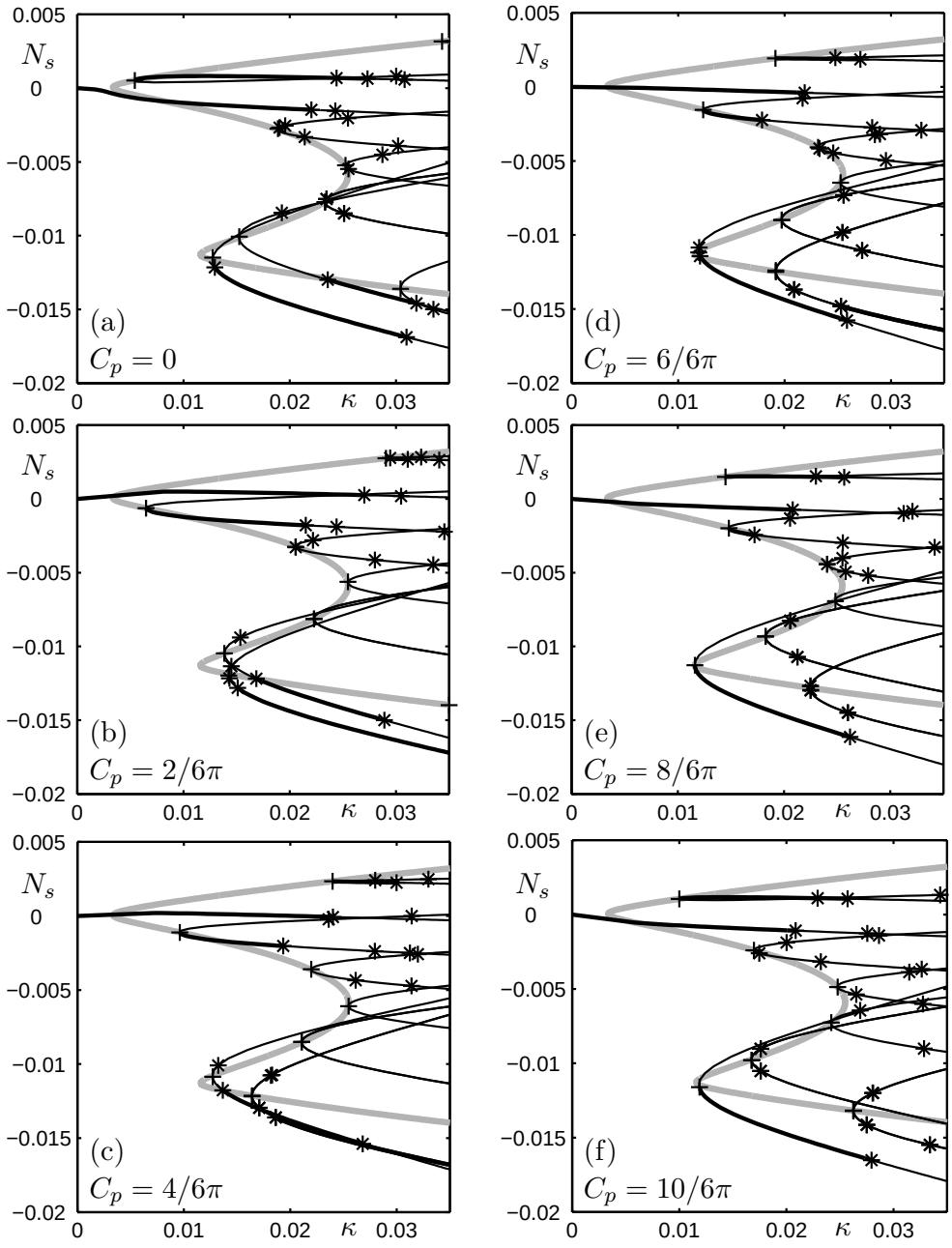

Figure 5. The EFMs for negative detuning $\Delta = -0.0595$ in the (κ, N_s)-projection for different values of the feedback phase C_p as indicated in the panels. Stable parts of the branches are plotted thick, saddle-node bifurcations are indicated as plusses (+) and Hopf bifurcations by stars (∗); the gray curve is traced out by the saddle-node bifurcations as C_p is changed.

entire saddle-node curve with a single EFM branch C_p needs to be varied over approximately 16π.

Figure 5 shows the situation for a negative detuning of $\Delta = -0.0595$. Now the EFMs around the filter center can be found in the low-inversion part of the (κ, N_s)-plane. Apart from this difference, the structure is very similar to the situation for positive detuning. However there are significant differences regarding the stability of the EMFs as will be discussed in the next section. The fact that respective panels of Fig. 4 and Fig. 5 are not each others symmetric images is again due to the influence of α.

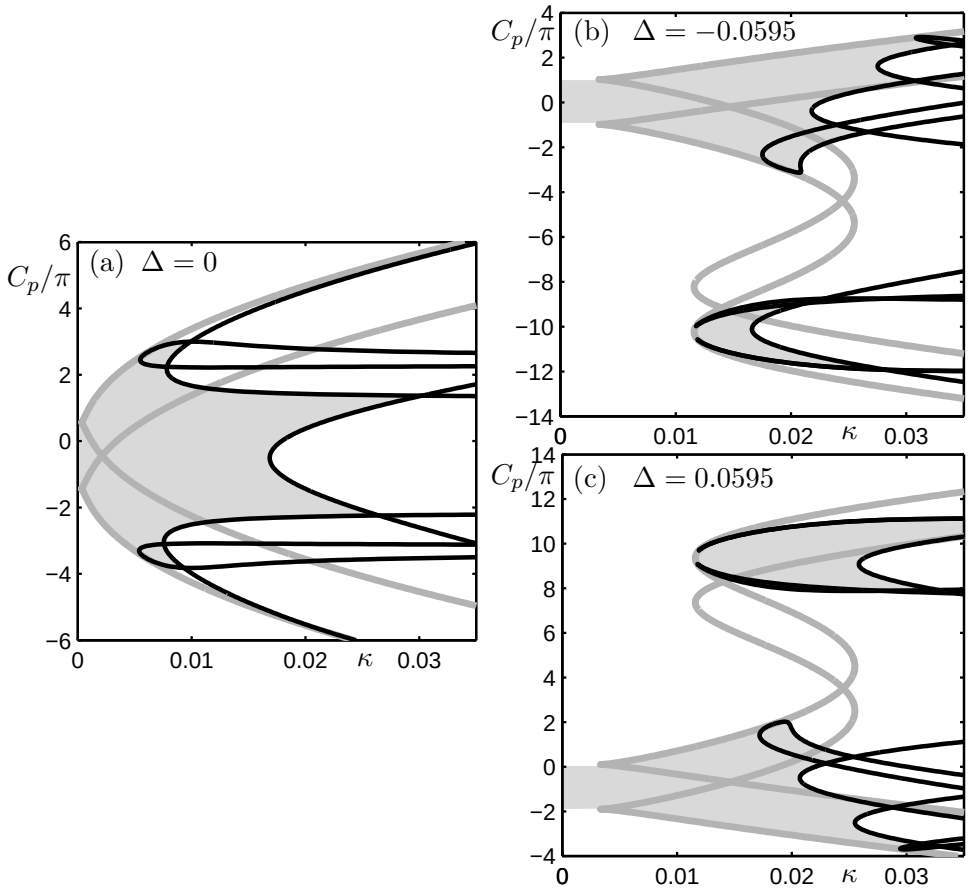

Figure 6. Two parameter bifurcation digram in the complex feedback plane (κ, C_p) for three different values of detuning indicated in the panels. The gray lines are saddle-node bifurcations and the black lines are Hopf bifurcations. In the light gray regions EFMs are stable.

5. STABILITY REGIONS OF EFMS

Figure 6 shows the stability of the EFMs in the (κ, C_p)-plane for three different values of the detuning Δ. In the gray regions the EFMs are stable. These regions are bounded by curves of saddle-node bifurcations (gray) and by curves of Hopf bifurcations (black). Shown is the stability region of the EFM that can be continued from the solitary laser state for C_P around zero. The panels show the respective regions over suitably many multiples of π in C_p. In fact, all 2π copies of these regions and curves coexist, leading to a large degree of multistability.

Figure 6(a) shows the situation for zero detuning. There is a single large region of stable EFMs. It is bounded to the left (decreasing κ) by saddle-node bifurcations. To the right it is bounded by different Hopf bifurcation curves. Crossing the middle Hopf curve (around $C_p = 0$) leads to relaxation oscillations. However, crossing the lower and upper Hopf curves leads to frequency oscillations, which were first reported in Ref. [8]. Frequency oscillations are round-trip oscillations in the feedback loop and, therefore, have a period on the order of the delay time τ. Remarkably, these round-trip oscillations have almost constant intensity in large regions where they are stable [10].

Figure 6(b) shows the situation for a negative detuning of $\Delta = -0.0595$. For this level of detuning two regions of stable EFMs exist: one stability region around the solitary laser state (around $C_p = 0$) and a second, smaller stability region one around the center frequency of the filter (around $C_p = -10\pi$). The Hopf bifurcation curve that forms the right-hand boundary of the region of stable EFMs around the filter center leads

to relaxation oscillations. On the other hand, the Hopf bifurcation curves that form the right-hand boundary of the larger stability region (around the solitary laser state) give rise to frequency oscillations. In fact, one finds frequency oscillations also in the region between both stability regions.

Figure 6(c) shows the situation for a positive detuning of $\Delta = 0.0595$. The situation is very similar to that shown in Fig. 6(b). There are two regions of stable EFMs, but now the one around the center frequency of the filter appears on the other side (with respect to C_p) of stability region around the solitary laser state (which again is located around $C_p = 0$). As before, we find relaxation oscillations to the right of the smaller stability region, while in the area to the right of the larger region (around the solitary laser state) and betwen the two EFM stability regions we find frequency oscillations. However, there is a difference between positive and negative detunings. Notice that the EFM stability region around the center frequency of the filter (around $C_p = 10\pi$) is noticeably larger than in the case of negative detuning. This means that a much higher feedback rate κ is necessary to destabilize these EFMs and, hence, to encounter relaxation osciallations.

We remark that the stability regions of relaxation and frequency oscillations are bounded by further bifurcations, namely, saddle-node bifurcations of limit cycles, period-doublings and torus bifurcations. A detailed analysis of these stability regions of oscillations is beyond the scope of this paper and will be discussed elsewhere.

6. CONCLUSIONS

We showed a comprehensive picture of the mode structure of a semiconductor laser with filtered optical feedback. These modes — the external filtered modes — are organized by saddle-node bifurcations and Hopf bifurcations. As the feedback rate is increased new EFMs are born in saddle-node bifurcation and then destabilize in Hopf bifurcations. When the detuning between the laser and the filter is increased one finds two separated EFM components, which both feature stable EFMs. When shown in the plane of feedback rate against feedback phase, the two different regions of stable EFMs give rise to relaxation oscillations and frequency oscillations, respectively, when the EFMs destabilize for larger values of the feedback rate. Generally speaking, relaxation oscillations are found stably for high feedback rates around the filter center. Frequency oscillations, on the other hand, already exists for lower values of the feedback rate around the solitary laser state.

Further analysis of these frequency oscillations and their characteristics is the subject of ongoing research. This involves possible connections between relaxation oscillations and frequency oscillations and an experimental verification of the rate equation based bifurcation analysis.

REFERENCES

1. G. van Tartwijk and D. Lenstra, "Semiconductor lasers with optical injection and feedback," *Quantum Semiclass. Opt.* **7**, pp. 87–143, 1995.
2. S. Wieczorek, B. Krauskopf, T. Simpson, and D. Lenstra, "The dynamical complexity of optically injected semiconductor lasers," *Physics Reports* **416(1-2)**, pp. 1–128, 2005.
3. B. Krauskopf and D. L. (Eds.), *Fundamental Issues of Nonlinear Laser Dynamics*, AIP Conference Proceedings Vol. 548, Melville, New York, 2000.
4. B. Krauskopf, "Bifurcation analysis of lasers with delay," in *Unlocking Dynamical Diversity: Optical Feedback Effects on Semiconductor Lasers*, D. Kane and K. Shore, eds., pp. 147–183, Wiley, (New York), 2005.
5. D. Lenstra and M. Yousefi, "Theory of delayed optical feedback in lasers," in *Fundamental Issues of Nonlinear Laser Dynamics*, B. Krauskopf and D. Lenstra, eds., *AIP Conference Proceedings* **548**, pp. 66–86, (New York), 2000.
6. D. Lenstra, G. Vemuri, and M. Yousefi, "Generalized optical feedback," in *Unlocking Dynamical Diversity: Optical Feedback Effects on Semiconductor Lasers*, D. Kane and K. Shore, eds., pp. 55–80, Wiley, (New York), 2005.
7. A. Fischer, O. Andersen, M. Yousefi, S. Stolte, and D. Lenstra, "Experimental and theoretical study of filtered optical feedback in a semiconductor laser," *IEEE J. Quantum Electron.* **36**, pp. 375–384, 2000.

8. A. Fischer, M. Yousefi, D. Lenstra, M. Carter, and G. Vemuri, "Experimental and theoretical study of semiconductor laser dynamics due to filtered optical feedback," *Phys. Rev. Lett.* **92**, pp. 023901–023904, 2004.
9. M. Yousefi, D. Lenstra, and G. Vemuri, "Nonlinear dynamics of a semiconductor laser with filtered optical feedback and the influence of noise," *Phys. Rev. E* **67**, p. 046213, 2003.
10. H. Erzgräber, B. Krauskopf, and D. Lenstra, "Frequency versus relaxation oscillations in a semiconductor laser with coherent filtered optical feedback," *Applied Nonlinear Mathematics Research Report, University of Bristol* **2005.24**, 2006.
11. M. Nizette and T. Erneux, "Semiconductor lasers subject to weak filtered optical feedback: an analytical study," submitted.
12. K. Green and B. Krauskopf, "Mode structure of a semiconductor laser subject to filtered optical feedback," *Opt. Commun.* **258(2)**, pp. 243–255, 2006.
13. K. Green and B. Krauskopf, "Analysis of the external filtered modes of a semiconductor laser with filtered optical feedback," *in: Semiconductor Lasers and Laser Dynamics II, Proceedings of SPIE (D. Lenstra, M. Pessa and Ian H. White; Eds.)* **6184 (30)**, 2006.
14. K. Engelborghs, T. Luzyanina, and G. Samaey, *DDE-BIFTOOL v. 2.00 user manual: a Matlab package for bifurcation analysis of delay differential equations. Technical report TW-330*, Department of Computer Science, K.U. Leuven, Leuven, Belgium, 2001.